



## Mode-selective few-mode Brillouin fiber lasers based on intramodal and intermodal SBS

NING WANG,<sup>1</sup> J. C. ALVARADO-ZACARIAS,<sup>1</sup> MD SELIM HABIB,<sup>1,2</sup>  HE WEN,<sup>1</sup>   
 J. E. ANTONIO-LOPEZ,<sup>1</sup> PIERRE SILLARD,<sup>3</sup> A. AMEZCUA-CORREA,<sup>3</sup> AXEL SCHÜLZGEN,<sup>1</sup>  
 R. AMEZCUA-CORREA,<sup>1</sup> AND GUIFANG LI<sup>1,\*</sup>

<sup>1</sup>CREOL, The College of Optics and Photonics, University of Central Florida, Orlando, Florida 32816, USA

<sup>2</sup>Department of Electrical and Computer Engineering, Florida Polytechnic University, Lakeland, Florida 33805, USA

<sup>3</sup>Prysmian Group, Parc des Industried Artois Flandres, Haisnes Cedex, 62092, France

\*Corresponding author: li@creol.ucf.edu

Received 17 December 2019; revised 10 March 2020; accepted 15 March 2020; posted 18 March 2020 (Doc. ID 385444); published 9 April 2020

**Mode-selective fiber lasers have advantages in a number of applications. Here we propose and experimentally demonstrate a transverse mode-selective few-mode Brillouin fiber laser using the mode-selective photonic lantern. We generated the lowest three orders of linearly polarized (LP) modes based on both intramodal and intermodal stimulated Brillouin scattering (SBS). Their slope efficiencies, optical spectra, mode profiles, and linewidths were measured.** © 2020 Optical Society of America

<https://doi.org/10.1364/OL.385444>

Stimulated Brillouin scattering (SBS) is one of the prominent nonlinear effects in optical fibers. It can be described as a nonlinear interaction between the pump and Stokes wave mediated by the acoustic wave [1]. A Brillouin fiber laser (BFL) could be realized in a ring cavity by using SBS to provide gain for the signal traveling in the backward direction [2,3]. There are a number of advantages of BFLs. For example, the optical signal-to-noise ratio (OSNR) of a BFL is much higher than the pump laser due to the stronger damping of the acoustic field compared to the optical field [4,5]. Also, BFLs have attracted interests due to their ultranarrow linewidth [6,7]. A BFL with a linewidth of tens of hertz has been experimentally demonstrated [8], which can be, in turn, used for high-quality microwave signal generation [9,10]. Based on cascaded SBS processes, multiple wavelengths could be generated in a single ring cavity [11,12].

Lasers of high-order mode (HOM) have been extensively investigated in recent years because of their advantages in a number of applications, including fiber sensing [13], microscopy imaging [14], laser material processing [15], and gravitational wave detection [16]. Several techniques have been proposed to construct HOM fiber lasers. By using a rare-Earth-doped few-mode fiber (FMF) with intracavity mode-selective elements, it is possible to generate a specific linearly polarized (LP) mode. The HOM lasers at different wavelengths in ytterbium- [17], erbium- [18], and thulium-doped fiber [19] have been experimentally demonstrated. Recently, an LP<sub>01</sub>/LP<sub>11</sub> mode BFL

based on only intramodal SBS has been reported [20]. However, intermodal SBS caused the degradation of laser mode purity.

In this work, we demonstrate, for the first time, an intracavity transverse mode-selective BFL based on intermodal SBS effect with the fundamental mode as the pump. A pair of mode-selective photonic lanterns (MSPLs) was placed inside the ring cavity to act as spatial mode filters. In this configuration, pump mode converters are not necessary. For comparison, we also generated the BFLs of the three lowest-order LP modes based on the intramodal SBS effect. The slope efficiencies, mode intensity profiles, optical spectra, and linewidths were characterized for both cases.

The FMF used in our experiment is the four-LP mode FMF made by Prysmian Group. Its refractive index profile is shown in Fig. 1(a), and its cross-sectional microscope image is shown in Fig. 1(b). It is a step-index fiber with a core and cladding diameter of 15.2 μm and 125 μm, respectively. The numerical aperture (NA) was measured to be 0.17, ensuring it supports six LP modes at a wavelength of 1550 nm. We calculated the transverse field distributions of the six LP modes supported by this FMF at 1550 nm by COMSOL, the results are shown in Fig. 1(c). We also computed the guided acoustic modes of the fiber at a frequency of 10.6 GHz, which is the Brillouin frequency shift for the backward SBS. Figure 1(d) shows the material density vibration fields of the 10 lowest orders of longitudinal acoustic modes guided in the core area. It should be noted that the number of guided acoustic modes of the same fiber is much larger than that of the optical modes [21].

Both intramodal and intermodal SBS will occur in the FMF once the field distribution of the acoustic wave is matched with the pump and scattered waves. The Brillouin gain spectrum is a combination of gain peaks generated by each guided acoustic mode [22],

$$g(\Omega) = \sum_m g_{0m} \frac{\left(\frac{\Gamma_B}{2}\right)^2}{(\Omega - \Omega_m)^2 + \left(\frac{\Gamma_B}{2}\right)^2}, \quad (1)$$

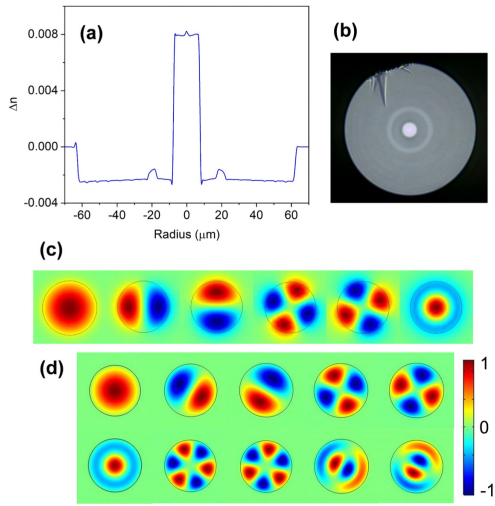


**Fig. 1.** (a) Measured refractive index profile and (b) cross-sectional microscope image of the four-LP mode FMF; (c) calculated optical fields of the six LP modes supported by the FMF; (d) field distributions of the 10 lowest-order guided acoustic modes.

**Table 1. Overlap Integrals of Normalized Acoustic and Optic Fields that Form the Main Brillouin Gain Peaks**

	LP <sub>01,s</sub>	LP <sub>11,s</sub>	LP <sub>21,s</sub>
LP <sub>01,p</sub>	$9.15 \times 10^4$	$7.76 \times 10^4$	$6.56 \times 10^4$
LP <sub>11,p</sub>	—	$7.15 \times 10^4$	—
LP <sub>21,p</sub>	—	—	$5.47 \times 10^4$

where  $\Omega_m$  is the acoustic frequency of the  $m$ th guided acoustic mode;  $\Gamma_B$  is the acoustic damping rate;  $g_{0m}$  is the gain coefficient, which is proportional to the square of the field overlap integral between the two optic fields and one acoustic field. The overlap integral can be expressed as

$$\eta_{ijm} = \iint \varphi_{i,p} \xi_m \varphi_{j,s}^* ds, \quad (2)$$

where  $\varphi_{i,p}$  and  $\varphi_{j,s}$  mean the normalized field distribution of the  $i$ th pump wave and  $j$ th Stokes wave, and  $\xi_m$  is the normalized field distribution of the  $m$ th guided acoustic mode. We found that the Brillouin gain coefficients mediated by the higher-order acoustic modes would be much smaller, because their higher spatial frequencies decrease the field overlap with the optical modes.

Here we calculated the value of  $\eta_{ijm}$  for different pump and Stokes wave pairs associated with the acoustic mode that provides the highest Brillouin gain, as shown in Table 1. We can find that for HOM signals, the overlap between the optical and acoustic fields for intermodal SBS (pump at LP<sub>01</sub> mode) are better compared to the intramodal SBS.

We used a pair of 6-to-1 MSPLs to realize the LP mode conversion between the single-mode fiber (SMF) and the FMF. MSPLs are passive all-fiber devices that contain a set of input SMFs and one FMF output, as shown in Fig. 2(a). We used dissimilar SMFs as the input to obtain the mode-selective fashion [23]. Figure 2(b) shows the cross-sectional image of the end of a six-mode MSPL, and the resulting FMF has a core and cladding

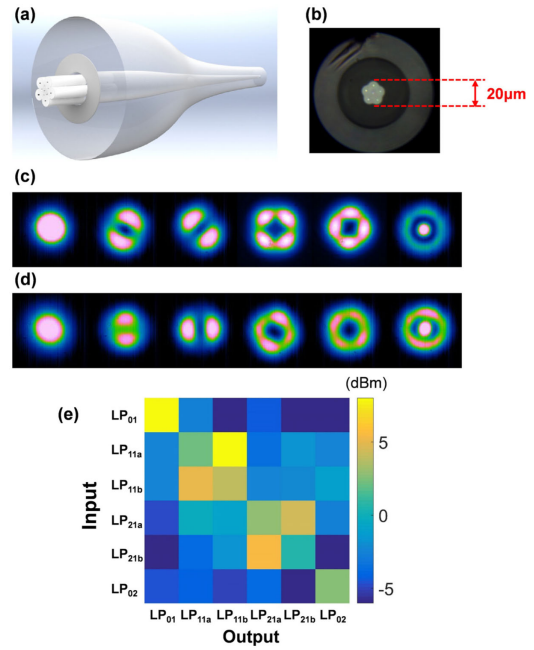


**Fig. 2.** (a) Schematic view of the structure of a MSPL, (b) cross-sectional microscope image of the end of a six-mode MSPL; output mode intensity profiles of (c) MSPL1 and (d) MSPL2 measured at 1550 nm; (e) mode transfer matrix of the pair of MSPLs with 1 km of FMF.

diameter of 20  $\mu\text{m}$  and 110  $\mu\text{m}$ , respectively. The output facet of the MSPL can be easily spliced with a four-LP mode FMF. We fabricated two six-mode MSPLs, denoted MSPL1 and MSPL2, and measured their output mode profiles using a laser with a wavelength of 1550 nm. Figures 2(c) and 2(d) show the output mode profiles of MSPL1 and MSPL2, respectively. The six lowest-order LP modes were clearly observed with a mode conversion efficiency of  $\sim 70\%$ . We also measured the mode transfer matrix from MSPL1 to MSPL2 with 1 km of FMF between them, and the result is shown in Fig. 2(e). The mode selectivity between different mode groups was around 7 dB, but the selectivity within the same mode group was much lower due to the orientation of the degenerate modes rotating within the circular core of the FMF. The total link losses for the LP<sub>01</sub>, LP<sub>11</sub>, LP<sub>21</sub>, and LP<sub>02</sub> modes were measured to be 3.2 dB, 4.3 dB, 6.7 dB, and 9.5 dB, respectively.

The experimental setup for the transverse mode-selective BFLs is shown in Fig. 3. The pump was a tunable laser source (TLS) with a wavelength of 1550 nm, amplified by an erbium-doped fiber amplifier (EDFA). For intramodal Brillouin lasing, the pump traveled through the circulator and was launched into MSPL2 to create the desired LP mode. The output of MSPL2 was spliced to 1 km of the four-LP mode FMF. The backscattered Stokes wave of the same mode went through the circulator from port 2 to port 3, and was injected into MSPL1 with the port mapping to the same LP mode. The HOM signal from MSPL1 was collimated and coupled back into the 1 km FMF with a pair of 20X objective lenses, and circulated clockwise as shown by the red arrow. The fiber coupling losses were less than 1 dB for all LP modes, and each objective lens introduced an additional 1 dB loss. For the intermodal Brillouin lasing, the pump was directly launched into the LP<sub>01</sub> port of MSPL2. The

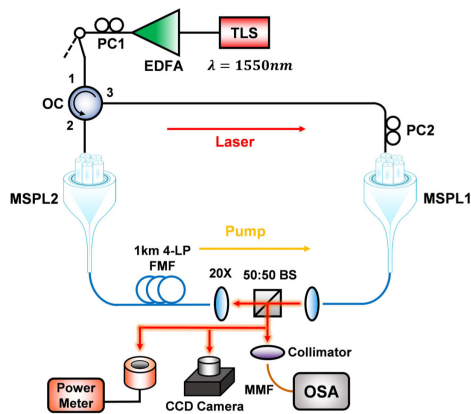


**Fig. 3.** Experimental setup for the mode-selective few-mode BFLs.

ports corresponding to the desired HOM for both MSPLs were connected to ports 2 and 3 of the circulator. Due to intermodal SBS effects, all LP modes are scattered backward even with only the fundamental mode as the pump. However, only the selected HOM can pass through the MSPL and oscillate inside the ring cavity. The laser came out from a 3 dB beam splitter (BS). The laser power and mode profiles were measured by a power meter and a charge-coupled device (CCD) camera. We also coupled the laser into a piece of multimode fiber, after which its optical spectra were observed using an optical spectrum analyzer (OSA). Two SMF polarization controllers (PCs) were used to optimize the polarization states of the pump and Stokes waves, in order to maximize the Brillouin gain.

We measured the laser power of the  $LP_{01}$ ,  $LP_{11}$ , and  $LP_{21}$  modes based on both intramodal and intermodal SBS, as shown in Fig. 4(a). The results indicate that for all cases, lasing started after the pump power exceeded their threshold values, and over 24 mW of laser power was observed. The  $LP_{01}$  lasing mode had the highest laser power and lowest threshold pump value. Its threshold pump power was 40 mW, and the slope efficiency was 11.6%. The low slope efficiency was partly due to polarization state misalignment between the pump and Stokes wave. Another reason was the relatively large insertion losses of the MSPLs. The slope efficiencies for  $LP_{11}$  SBS lasing modes based on intramodal and intermodal SBS were 10.9% and 8.9%, respectively. The values for  $LP_{21}$  lasing modes based on intramodal and intermodal SBS were 10.5% and 8.6%, respectively. The lower laser power of the HOMs was mainly caused by a larger insertion loss of the photonic lantern pair compared to the  $LP_{01}$  mode, and also the smaller overlap integral between the optical and guided acoustic fields. From Fig. 4(a), the laser power of HOMs based on intermodal SBS was always smaller than that based on intramodal SBS, although their Brillouin gain coefficients are larger according to Table 1. This was because the strong backward SBS of the fundamental mode consumed part of the pump power. The polarization misalignment was another reason. The measured mode intensity profiles of BFLs of different LP modes based on intramodal SBS and intermodal SBS configuration are shown in Figs. 4(b) and 4(c), respectively. We can see that their mode patterns are nearly ideal, and the mode purities were over 90% for all cases thanks to the high mode selectivity of the MSPLs.

We measured the optical spectra of all the SBS lasing modes using an OSA (Ando AQ-6315e). The results are shown in

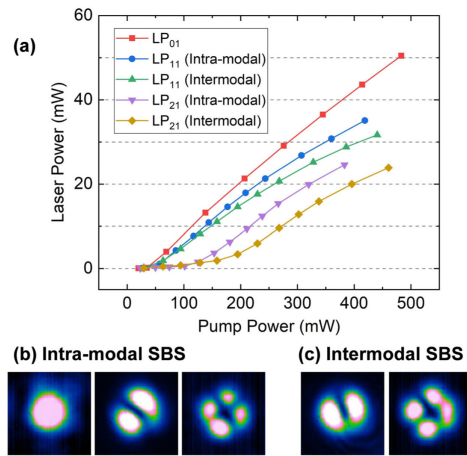


**Fig. 4.** (a) Output laser power versus pump power for each LP lasing mode based on intramodal and intermodal SBS, measured mode intensity profiles of the few-mode BFLs based on (b) intramodal SBS and (c) intermodal SBS.

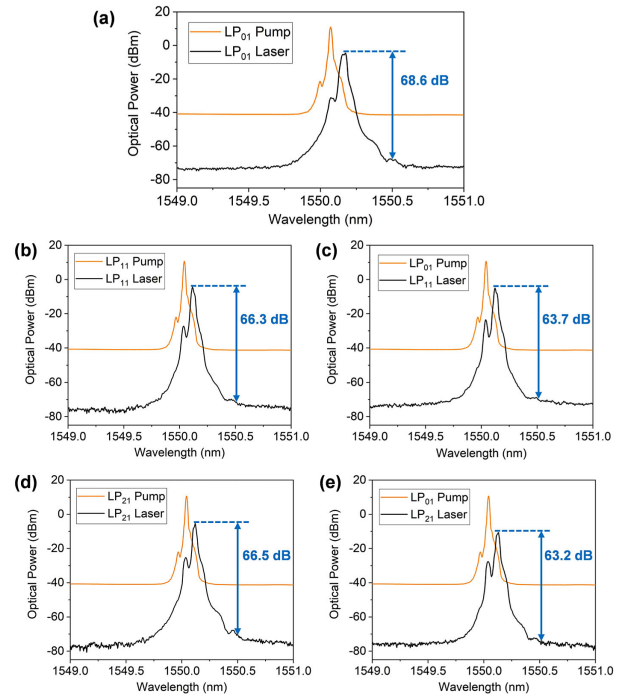


**Fig. 5.** Optical spectra of the SBS lasing modes for (a)  $LP_{01}$  mode;  $LP_{11}$  modes based on (b) intramodal and (c) intermodal SBS;  $LP_{21}$  modes based on (d) intramodal and (e) intermodal SBS.

Fig. 5. The resolution of the OSA was set to be 0.02 nm. The optical spectra of the  $LP_{01}$  mode BFL and pump are shown in Fig. 5(a). The frequency downshift between the pump and the laser was around 0.1 nm, corresponding to a Brillouin frequency downshift of 10.6 GHz. There is a small peak in the laser spectra that came from the reflection of the residual pump at the end of the FMF. It can be suppressed by angle cleaving the FMF ends. The OSNR was measured to be 68.6 dB, nearly 20 dB higher than that of the pump. Figures 5(b) and 5(c) indicate the results for  $LP_{11}$  lasing modes based on intramodal and intermodal SBS, respectively. The shapes of their optical spectra look similar, and

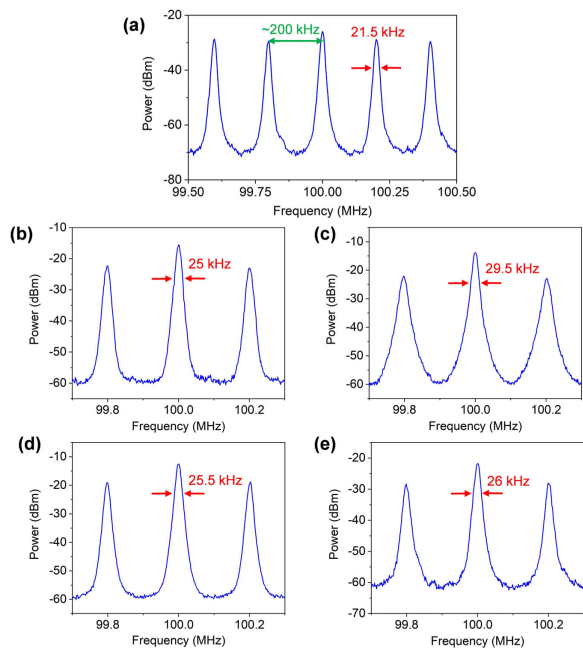


**Fig. 6.** Beat-note spectrum of self-heterodyne linewidth measurement for (a)  $LP_{01}$  mode;  $LP_{11}$  mode based on (b) intramodal and (c) intermodal SBS;  $LP_{21}$  mode based on (d) intramodal and (e) intermodal SBS.

the OSNRs were measured to be 66.3 and 63.7 dB. The results of  $LP_{21}$  lasing modes based on intramodal and intermodal SBS are shown in Figs. 5(d) and 5(e), respectively, and their OSNRs were measured to be 66.5 and 63.2 dB.

We also investigated the linewidth of each generated few-mode BFLs using self-heterodyne measurements [24]. We employed a 90:10 fiber coupler to let a small part of the laser get out at the SMF side before it went through MSPL1. The laser was then separated into two arms using a 3 dB coupler. One arm traveled through 25 km of SMF for the decorrelation, and the other arm was shifted by 100 MHz using an acousto-optic modulator. The beat-note spectrum was recorded using an electrical spectrum analyzer (hp ESA-L1500A), and the resolution of the ESA was fixed to be 1 kHz. Figure 6(a) shows the beat-note spectrum for the  $LP_{01}$  mode BFL. There are multiple longitudinal modes observed with a spacing of around 200 kHz, which agrees well with the theoretical value. The 10 dB linewidth of the beat-note signal was around 21.5 kHz, after fitting with the Lorentzian shape, corresponding to a 3 dB laser linewidth, which was 3.6 kHz. The laser linewidth was narrowed by nearly 2 orders of magnitude compared to the pump, which is  $\sim 200$  kHz. The measured beat-note spectrum of  $LP_{11}$  lasing modes based on intramodal and intermodal SBS is shown in Figs. 6(b) and 6(c), and their 3 dB linewidths were 4.17 kHz and 4.9 kHz, respectively. The results of  $LP_{21}$  mode BFLs are shown in Figs. 6(d) and 6(e), and their 3 dB linewidths were 4.25 kHz and 4.33 kHz, correspondingly. It should be noticed that the intrinsic linewidths for all the LP modes were less than 100 Hz. Linewidth broadening was mainly caused by the instability of the environment, such as temperature fluctua-

tions and mechanical perturbations, which can be improved by better isolating the fiber from the environment.

In conclusion, a transverse mode-selective few-mode BFL was experimentally demonstrated in a 1 km four-LP mode FME. We generated the  $LP_{11}$  and  $LP_{21}$  lasing modes based on both intramodal and intermodal SBS effects. Over 24 mW of output laser power was observed for all the LP modes based on both intramodal and intermodal SBS, with slope efficiencies ranging from 8.5% to 11.6%. The mode intensity profiles were clearly observed. Their OSNRs ranged between 63.2 to 68.6 dB, and the 3 dB linewidths were around 4 kHz.

**Funding.** Army Research Office (W911NF-17-10553, W911NF-18-10365); National Science Foundation (ECCS-1808976, ECCS-1932858).

**Disclosures.** The authors declare no conflicts of interest.

## REFERENCES

1. A. Kobayakov, M. Sauer, and D. Chowdhury, *Adv. Opt. Photon.* **2**, 1 (2010).
2. D. R. Ponikvar and S. Ezekiel, *Opt. Lett.* **6**, 398 (1981).
3. L. Stokes, M. Chodorow, and H. Shaw, *Opt. Lett.* **7**, 509 (1982).
4. G. Wang, L. Zhan, J. Liu, T. Zhang, J. Li, L. Zhang, J. Peng, and L. Yi, *Opt. Lett.* **38**, 19 (2013).
5. J. Wang, Y. Hou, Q. Zhang, D. Jin, R. Sun, H. Shi, J. Liu, and P. Wang, *Opt. Express* **23**, 28978 (2015).
6. S. Smith, F. Zarinetchi, and S. Ezekiel, *Opt. Lett.* **16**, 393 (1991).
7. J. Geng, S. Staines, Z. Wang, J. Zong, M. Blake, and S. Jiang, *IEEE Photon. Technol. Lett.* **18**, 1813 (2006).
8. Z. Ou, X. Bao, and L. Chen, *IEEE Photon. Technol. Lett.* **26**, 2058 (2014).
9. J. Geng, S. Staines, and S. Jiang, *Opt. Lett.* **33**, 16 (2008).
10. J. Liu, L. Zhan, P. Xiao, G. Wang, L. Zhang, X. Liu, J. Peng, and Q. Shen, *IEEE Photon. Technol. Lett.* **25**, 220 (2013).
11. L. Zhan, J. Ji, J. Xia, S. Luo, and Y. Xia, *Opt. Express* **14**, 10233 (2006).
12. M. H. Al-Mansoori and M. A. Mahdi, *Opt. Express* **16**, 7649 (2008).
13. A. Van Newkirk, J. E. Antonio-Lopez, A. Velazquez-Benitez, J. Albert, R. Amezcua Correa, and A. Schülzgen, *Opt. Lett.* **40**, 5188 (2015).
14. B. Harke, J. Keller, C. K. Ullal, V. Westphal, A. Schönle, and S. W. Hell, *Opt. Express* **16**, 4154 (2008).
15. J. Hamazaki, R. Morita, K. Chujo, Y. Kobayashi, S. Tanda, and T. Omatsu, *Opt. Express* **18**, 2144 (2010).
16. S. Chelkowski, S. Hild, and A. Freise, *Phys. Rev. D* **79**, 122002 (2009).
17. B. Sun, A. Wang, L. Xu, C. Gu, Y. Zhou, Z. Lin, H. Ming, and Q. Zhan, *Opt. Lett.* **38**, 667 (2013).
18. N. Wang, J. A. Zacarias, J. E. Antonio-Lopez, Z. S. Eznaveh, C. Gonnet, P. Sillard, S. Leon-Saval, A. Schülzgen, G. Li, and R. Amezcua-Correa, *Opt. Express* **26**, 32777 (2018).
19. J. M. O. Daniel and W. A. Clarkson, *Opt. Express* **21**, 29442 (2013).
20. X. Heng, J. Gan, Z. Zhang, J. Li, M. Li, H. Zhao, Q. Qian, S. Xu, and Z. Yang, *Opt. Lett.* **43**, 4172 (2018).
21. R. Waldron, *IEEE Trans. Microwave Theory* **17**, 893 (1969).
22. L. Dong, *J. Lightwave Technol.* **28**, 3162 (2010).
23. A. Velazquez-Benitez, J. Alvarado, G. Lopez-Galmiche, J. Antonio-Lopez, J. Hernández-Cordero, J. Sanchez-Mondragon, P. Sillard, C. Okonkwo, and R. Amezcua-Correa, *Opt. Lett.* **40**, 1663 (2015).
24. W. Schmid, C. Jung, B. Weigi, G. Reiner, R. Michalzik, and K. J. Ebeling, *IEEE Photon. Technol. Lett.* **8**, 1288 (1996).